arXiv:1604.00472v1 [cond-mat.soft] 2 Apr 2016

Contact statistics highlight distinct organizing principles of proteins and RNA

Lei Liu[1] and Changbong Hyeon[1,*]

[1]*School of Computational Sciences, Korea Institute for Advanced Study, 85 Heogiro Dongdaemun-Gu, Seoul 02455, Republic of Korea*

Although both RNA and proteins have densely packed native structures, chain organizations of these two biopolymers are fundamentally different. Motivated by the recent discoveries in chromatin folding that interphase chromosomes have territorial organization with signatures pointing to metastability, we analyzed the biomolecular structures deposited in the Protein Data Bank and found that the intrachain contact probabilities, $P(s)$ as a function of the arc length s, decay in power-law $\sim s^{-\gamma}$ over the intermediate range of s, $10 \lesssim s \lesssim 110$. We found that the contact probability scaling exponent is $\gamma \approx 1.11$ for large RNA ($N > 110$), $\gamma \approx 1.41$ for small sized RNA ($N < 110$), and $\gamma \approx 1.65$ for proteins. Given that Gaussian statistics is expected for a fully equilibrated chain in polymer melts, the deviation of γ value from $\gamma = 1.5$ for the subchains of large RNA in the native state suggests that the chain configuration of RNA is not fully equilibrated. It is visually clear that folded structures of large sized RNA ($N \gtrsim 110$) adopt crumpled structures, partitioned into modular multi-domains assembled by proximal sequences along the chain, whereas the polypeptide chain of folded proteins looks better mixed with the rest of the structure. Our finding of $\gamma \approx 1$ for large RNA might be an ineluctable consequence of the hierarchical ordering of the secondary to tertiary elements in the folding process.

RNA and proteins, under an appropriate environmental conditions, adopt three-dimensionally compact native folds that are essential for a variety of biological functions. Despite general similarities of the folding principles that both biopolymers are made of sequences foldable to a functionally competent structure as an outcome of evolutionary selection [1–5], the overall shape of the native RNA differs from that of proteins in several aspects. Proteins are in general more compact, globular, and flexible than RNA [6]. Such differences may be originated from distinct nature of building block. The energy scale of binary interaction that pairs nucleotides is typically greater than that of amino acids. Furthermore, the requirement of charge neutralization (or screening) along the backbone differentiates the foci of RNA dynamics, especially at the early stage of folding [7], from those of proteins.

Spotlighted in the recent studies of chromatin folding exploiting fluorescence in-situ hybridization (FISH) [8, 9] and chromosome conformation capture techniques [10–12], human chromosomes in the interphase have a territorial organization [9] and the individual chromosome is also partitioned into a number of topologically associated domains (TADs), possibly mediated by proteins such as CTCF and cohesin [13]. The contact probability $P(s)$ of two loci separated by the genomic distance s can provide glimpses into the arrangement of chromatin chain. From the polymer perspective, a test chain in a "fully" equilibrated homogeneous polymer melt is expected to obey the Gaussian statistics because of the screening of excluded volume interaction [14], thus satisfying $P(s) \sim s^{-3/2}$. It was, however, shown that $P(s)$ of human chromatin in cell nucleus displays $P(s) \sim s^{-1.08}$ at the genomic scales of $1 < s < 10$ Mb [11]. To account for the origins of the human genome organization and its characteristic scaling exponent $\gamma = 1.08$ and patterns of contact map demonstrating TADs, several different models have been put forward, which include the crumpled (fractal) globule [11, 15, 16], random loop [17], strings and binders switch model [18], and confinement-induced glassy dynamics [19].

Besides the overall shape, chain organizations of the native folds of RNA and proteins are in general visually different from each other. Compared with proteins in which α-helices, β-strands, and loops thread through one another to form a native structure, a folded RNA with large N looks more crumpled; a number of secondary structure elements (helices, bulges, loops) forming *independently stable* modular contact domains are further assembled into a compact three dimensional structure. Here, borrowing the several statistical measures that have been used to study the genome/chromosome organization inside cell nucleus, we substantiate the fundamental differences between the chain organizations of RNA and proteins in native states and discuss its significance in connection to their folding mechanisms.

METHODS

Calculation of contact probability and extraction of scaling exponent. Using atomic coordinates of RNA and protein from Protein Data Bank (PDB), we consider that two residues i and j are in contact if the minimum distance between any two heavy atoms

of these residues, located at $\vec{r}_i$ and $\vec{r}_j$, is smaller than a cut-off distance d_c (= 4 Å). The contact probability for a biomolecule α with chain length N_α (the number of residues) is thus determined by calculating

$$P_\alpha(s) = \frac{\sum_{i<j}^{N_\alpha} \delta(|i-j|-s)\Theta(d_c - \min|\vec{r}_i - \vec{r}_j|)}{\sum_{i<j}^{N_\alpha} \delta(|i-j|-s)}, \quad (1)$$

where $\Theta(x) = 1$ for $x \geq 0$; otherwise $\Theta(x) = 0$. Two examples of $P(s)$ are given in Figs.1B and 1C. The power law relation of $P(s) \sim s^{-\gamma}$ is observed over the intermediate scale. We determined the value of γ by fitting $P(s)$ over the range of $s_{\min} < s < s_{\max}$. The details of fitting procedure are discussed in the Supporting Material.

Mean contact probability. Each structure in the PDB has different chain size N_α ($\alpha = 1, 2, \ldots, I_{\max}$). Thus, to consider the non-uniform distribution of chain size in computing the mean contact probability, we calculated the following N-dependent probability averaged over the total number of distinct chain sizes:

$$\langle \overline{P}(s) \rangle = \frac{1}{N_{\max} - N_{\min} + 1} \sum_{N=N_{\min}}^{N_{\max}} \overline{P}(s|N), \quad (2)$$

where $\overline{P}(s|N) \equiv \sum_{\alpha=1}^{I_{\max}} \delta(N_\alpha - N) P_\alpha(s) / \sum_{\alpha=1}^{I_{\max}} \delta(N_\alpha - N)$ is the mean contact probability for the structures with chain size N, and we used the value of $P_\alpha(s)$ only for the range of $4 \leq s \leq N_\alpha^{2/3}$. $\langle \overline{P}(s) \rangle$ for RNA and proteins are shown in Fig. 1D. $\langle M(s) \rangle$, $\langle n_s(s) \rangle$, $\langle \mathrm{DOP} \rangle$, $\langle \mathrm{DOS} \rangle$, and $\langle R(s) \rangle$ were calculated using similar definitions as Eq. 2. A cautionary note is in place. Unlike the contact probability exponent calculated for each macromolecular structure, these mean properties obtained by averaging over each ensemble of proteins and RNA are meant for understanding the general difference between RNA and proteins as two distinct classes of macromolecules.

RESULTS

Power-law exponent γ of contact probability. The contact probability $P(s)$ calculated for individual biopolymers (Eq.1) exhibit power-law decay over the intermediate range of s, $10 \lesssim s \lesssim \mathcal{O}(10^2)$ (the left panel of Figs.1B and 1C). The scaling exponent γ from the fit using $P(s) \sim s^{-\gamma}$ was obtained for each biopolymer (see text and Figs. S1–S4 in the Supporting Material for details, where we discussed the accuracy of obtaining γ and showed the error bar of γ for each macromolecule), and its distributions, $p(\gamma)$s, for RNA and proteins are contrasted in Fig. 1A. Proteins have $p(\gamma)$ broadly distributed from 0.5 to 2.5 centered around $\gamma \approx 1.5$, whereas $p(\gamma)$ for RNA is sharply peaked at $\gamma \approx 1.1$. No clear correlation is found between γ and the chain length (N) in proteins; however, in RNA while γ values are broadly distributed at small N, they are sharply centered around $\gamma \approx 1.1$ when $N \gtrsim 100$ (see also Fig. S6).

The distinct scaling exponents, $\gamma = 1.11$ for the $P(s)$ of 23S rRNA ($P(s)$ at the left corner of Fig. 1B) and $\gamma = 1.49$ for FhuA ($P(s)$ at the left corner of Fig. 1C), elicit special attention. The value of $\gamma \approx 1.0$, especially for large sized RNA arises from their characteristic chain organization: Similar to TADs in chromosomes, proximal sequences along the chain are stabilized by base pairing to form independently stable modular "contact domains", consisting of hairpin, bulges, and loops. Further assemblies among these contact domains are achieved by a number of tertiary interactions (base triples, kissing loops, coaxial stackings through ribose zipper, A-minor motif, and metal-ion interactions) [32, 33]. The abundance of distal contacts resulting from the hierarchical chain assembly likely contributes to the greater frequency of the long-range contacts, giving rise to $\gamma \approx 1.11$ for 23S rRNA on the scale of $10 \lesssim s \lesssim 300$ (see the next section). The distinct chain organizations of RNA and proteins become more evident when molecules are visualized using rainbow coloring scheme spanning the chain (Figs.1B and 1C). The overall chain topology of 23S rRNA resembles a crumpled globule [34, 35] that retains clearly demarcated contact domains held by distal inter-domain contacts. The territorial organization of contact domains made of proximal sequences is highlighted in large sized RNA structures (see the large and small subunit of rRNA in Fig. 1B).

In stark contrast to rRNA, typical proteins with $\gamma \approx 1.5$ (indexed with black labels from 1 to 5 in Figs.1A and 1C) retain chain conformations whose subchains look topologically more intermingled with the rest of the structure, lacking visually distinct domains of a similar color. The intermingled chain configurations of native proteins as well as the contact probability scaling exponent $\gamma \approx 1.5$ points to a configuration of equilibrium globule, which is also supported by the same conclusion reached by investigating the loop size distribution of native protein structures [36]. Of particular note are the proteins with $\gamma < 1.0$, which are found at the outliers of $p(\gamma)$. For example, $\gamma = 0.73$ is for chrondroitin sulfate ABC lyase I (the protein indexed with 6) [31], the chain configuration of which has clearly demarcated contact domains.

Instead of calculating the s-dependent contact

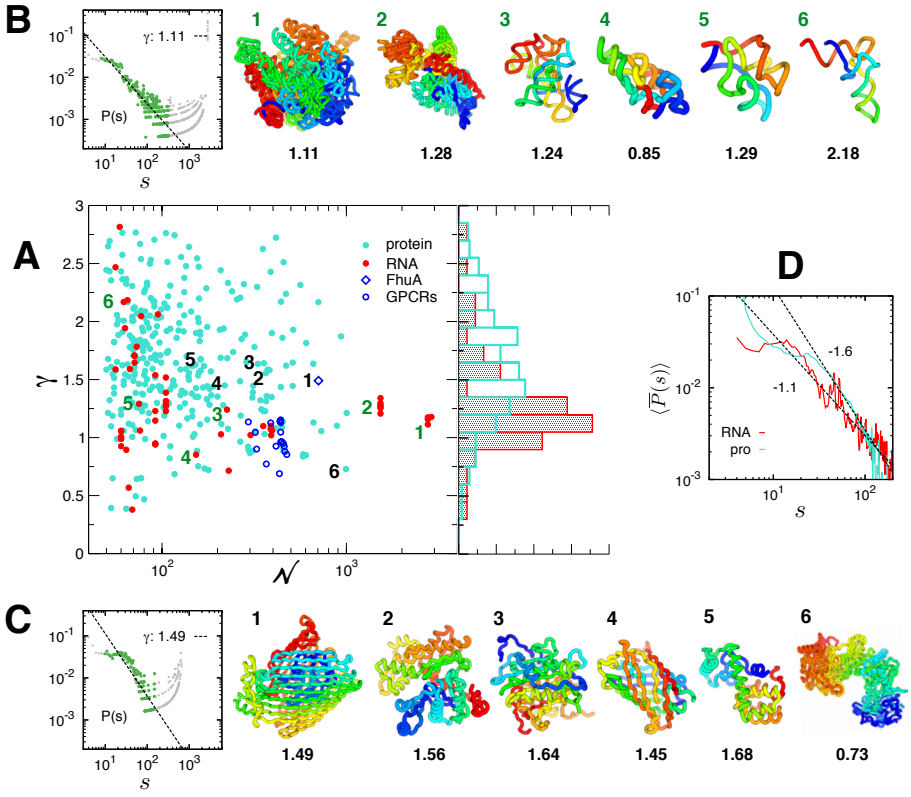

FIG. 1: Contact probability scaling exponent, γ, and chain configurations of RNA and proteins. **A.** γ versus N obtained for 60 individual RNA (data in red) and 324 proteins (data in cyan), whose γ value is obtained from the power-law fit to $P(s)$ with the correlation coefficient (c.c.) greater than > 0.9 (see Fig.S4 for γ vs. N plot with error bars, and Tables I, II in Supporting Material for PDB entries used here). The data points for FhuA and GPCRs are included for further discussion although c.c< 0.9. Histograms of γ, $p(\gamma)$ for RNA ($\gamma \approx 1.30 \pm 0.44$) and proteins ($\gamma = 1.65 \pm 0.50$) are shown on the right. **B.** Representative structures of RNA in rainbow coloring scheme from 5' (blue) to 3' (red), indexed with the number in γ vs. N plot. Depicted are the structures of **1.** a large subunit of rRNA (PDB entry: 2O45 [20], $\gamma = 1.11$), **2.** a small subunit of rRNA (2YKR, $\gamma = 1.28$) [21], **3.** Twort group I ribozyme (1Y0Q, $\gamma = 1.24$) [22], **4.** A-type ribonuclease P (1U9S, $\gamma = 0.85$) [23], and **5.** TPP-riboswitch (3D2G, $\gamma = 1.29$) [24]. $P(s)$, which provides γ value, is shown for a large subunit of rRNA on the left corner. The scaling exponent (γ) of $P(s) \sim s^{-\gamma}$ is obtained from the fit (dashed line) to the data points in green; the data in gray are excluded from the fit (see Supporting Material for details of fitting procedure). **C.** Protein structures in rainbow coloring scheme from the N- (blue) to C-terminus (red). Depicted in (C) are the structures of **1.** FhuA (1QJQ $\gamma = 1.49$) [25], **2.** an actin monomer (1J6Z $\gamma = 1.56$) [26], **3.** metacaspase (4AF8, $\gamma = 1.6$) [27], **4.** Green Fluorescent Protein (1EMA, $\gamma = 1.4$) [28], **6.** T4 lysozyme (2LZM, $\gamma = 1.7$) [29, 30], and **6.** Chondroitin Sulfate ABC lyase I (1HN0, $\gamma = 0.73$) [31]. $P(s)$ for FhuA is shown on the left corner. **D.** The mean contact probabilities, $\langle \overline{P}(s) \rangle$, calculated over the RNA and protein structures in the PDB.

probability for individual molecules ($P_\alpha(s)$, $\alpha = 1, 2, \ldots I_{\max}$), one can also consider ensemble averaged characteristics of native RNA and protein organizations, $\langle \overline{P}(s) \rangle$ (Eq.2, Fig.1 D). The mean contact probability calculated for each ensemble of RNA and proteins exhibits power-law decay $\langle \overline{P}(s) \rangle$ with $\gamma \approx 1.1$ for RNA and $\gamma \approx 1.6$ for proteins on the scale of $(20 - 30) \lesssim s \lesssim 100$, which helps us understanding the general difference of structural ensemble between RNA and proteins as two distinct classes of macromolecules.

Cautionary remarks are in place in regard to the power-law scaling of $P(s)$. The characteristic power-law decay behavior of 23S rRNA with $\gamma = 1.1$ is only valid for intermediate range of s. For small s, $P(s)$ decays with a different power-law exponent (see the

two panels of $P(s)$ in Figs. 1B and 1C). As reported by Lua and Grosberg [34], on local scales both RNA and proteins have a chain organization different from the one on larger scale, which is also confirmed in our study by the distinct scaling exponent $\gamma \approx 0.4$ for RNA and $\gamma \approx 1.4$ for proteins with $s < 20$ (Fig. S7). Hence, in the strict sense the chain organizations of both RNA and proteins are *not* scale-invariant, which is not the case for any real polymer, either. Depending on the length scale of interest, different picture is revealed from real polymer chains. Of note, the new scaling exponent $\gamma = 0.75$ recently discovered for chromatin organization at resolution (10 kb $\lesssim s <$ 1 Mb) [37] higher than the previous study ($s \gtrsim$ 700 kb) [11] implies that the self-similarity found at the intermediate resolution ($P(s) \sim s^{-1.08}$) cannot be extended to the internal structure of contact domain with $P(s) \sim s^{-0.75}$.

Long range contacts from contact map. Contact maps along with the three dimensional structure offer a more concrete insight into the distinct chain organization of biopolymers with different γ. For instance, the contact maps of 23S-rRNA ($\gamma = 1.11$) (Fig. 2A) and FhuA ($\gamma = 1.49$) (Fig. 2B) reveal that 23S rRNA has a greater density of long-range contacts than FhuA. Interestingly, in 23S rRNA the modular contact domains made of sequences, spanning $i = 500 - 1000$ (magenta) and $1500 - 1750$ (orange) or between $i = 500 - 1000$ (magenta) and $2000 - 2500$ (cyan), form extensive interfaces (Fig. 2A). In comparison, FhuA has β-barrel structure with the long-range tertiary contacts formed between the subdomain (blue) made of N-terminal sequences ($i = 1 - 150$) and β-strands ($i = 200 - 700$) surrounding it (Fig. 2B).

To generalize this finding for RNA and proteins, for each structure we calculated the proportion of long-range contacts (ϕ), between any sites i and j, satisfying $j - i \geq s_{\min}$, as the ratio between the observed number of long-range contacts and the maximum possible number of long-range contacts, i.e., $\phi = \mathcal{N} \sum_{j-i \geq s_{\min}}^{N} \Theta(d_c - |\vec{r}_i - \vec{r}_j|)$, where $\Theta(\cdots)$ is the Heaviside step function and the normalization constant $\mathcal{N} = (N - s_{\min} + 1)(N - s_{\min})/2$. The corresponding histograms $p(\phi)$ for RNA and proteins are shown in Fig. 2C with $s_{\min} = 30$. The finding that RNA has $p(\phi)$ distributed to larger ϕ values than proteins indicates that a significant number of tertiary contacts are used for assembling the secondary structure elements abundant in RNA. This result is robust to the variation of $s_{\min}$ value.

Inter-subchain interactions and surface roughness. In order to quantify further the distinct chain organization of RNA and proteins, we borrow analytic tools developed in the studies of chromosome organization [34, 35]. The number of contacts, $M(s)$, that a subchain has with the rest of the structure (see Fig. 3A) [16], scales as $\langle M(s) \rangle \sim s^{\beta_1}$ for both RNA and proteins, where $\langle \ldots \rangle$ denotes an average over the chain size frequency (see Materials and Methods). The exponent β_1 is different for RNA ($\beta_1^{\rm RNA} = 0.9$) and protein ($\beta_1^{\rm prot} = 0.6$), and $\langle M \rangle$ is greater for RNA when $s \gtrsim 40$, indicating that RNA has more number of inter-subchain contacts for $s \gtrsim 40$. The same conclusion was drawn by computing the "roughness" of the subchain surface [35], which is quantified using $n_{\rm s}(s)$, the number of monomers in a subchain that are in contact with at least one monomer belonging to other subchains (see Fig. 3B). $\langle n_s(s) \rangle_L \sim s^{\beta_2}$ with $\beta_2^{\rm RNA} = 0.9 > \beta_2^{\rm prot} = 0.7$, suggesting that RNA have rougher subchain surfaces. The scaling relationships of the inter-subchain interactions ($M \sim s^{0.9}$) and the surface monomers ($n_s \sim s^{0.9}$) for RNA compare well with those of crumpled globules (M, $n_s \sim s^1$) [16, 35].

$\langle M(s) \rangle$ and $\langle n_s(s) \rangle$ are related to each other with $\langle M(s) \rangle \approx Q \langle n_s(s) \rangle$ where $Q \sim s^{\nu d}/s$ is the proportionality constant, the total number of possible monomers ($\sim s^{\nu d}$) that can fill the volume defined by a blob consisting of s monomers, thus giving a scaling relation $\beta_1 = \nu d - 1 + \beta_2$ [35]. From this relation and $\beta_{1,2}$, we obtain the Flory exponent $\nu = 1/3$ for native RNA and $\nu = 0.3$ for proteins, which is in perfect agreement with the values of ν obtained from an independent analysis of macromolecular structures in the PDB, $\nu \approx 0.33$ for RNA and $\nu = 0.31$ for proteins in $R_G \sim N^{\nu}$ [6].

Degree of interpenetration and segregation. Next, we calculate the fraction of residues from other subchains found in the ellipsoidal volume enclosing a subchain averaged over all subchains of length s, which corresponds to the degree of interpenetration (DOP) [34]. The degree of segregation (DOS), DOS $= \langle d_{A,B}/(2R_G^{A \cup B}) \rangle$ is defined by the ratio between $d_{A,B}$ and $(2R_G^{A \cup B})$, where $d_{A,B}$ is the distance between the center positions of two non-overlapping subchains A and B, and $R_G^{A \cup B}$ is the gyration radius of the union of these two subchains. DOS is defined by the ratio of these two values ($d_{A,B}$ and $R_G^{A \cup B}$) averaged over all the pairs of subchains A and B with the same length s. DOP and DOS as a function of s for both RNA and proteins (Fig. 4) indicate that while subchains separated by a large arc length s are well separated from each other in RNA the subchains in RNA penetrate into other subchain's volume deeper than in proteins. This explains why the decline of $P(s)$ for RNA is slower than for

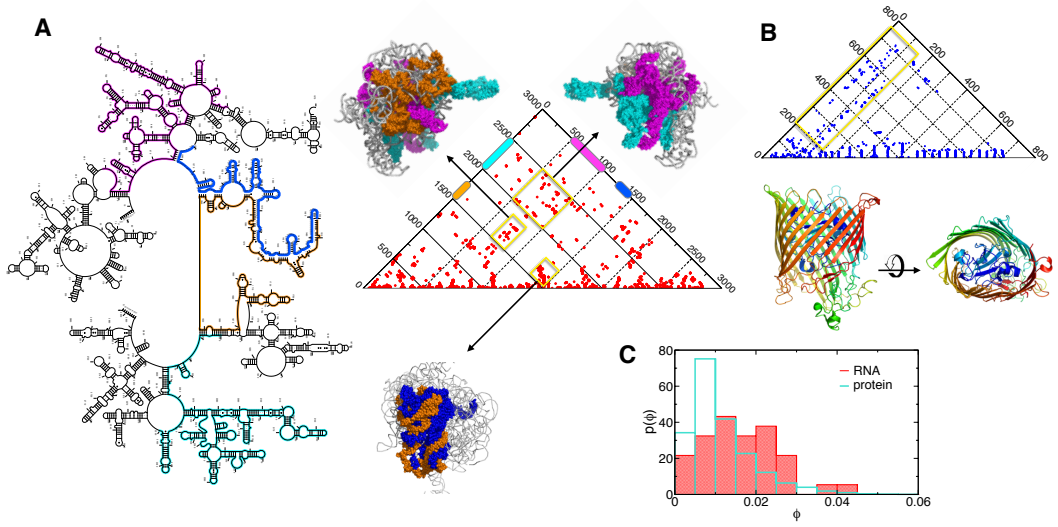

FIG. 2: Analysis of long-range contacts. **A**, **B**. Contact maps of 23S rRNA and FhuA, whose $P(s)$ are provided in Fig. 1. In FhuA, the long-range contacts ($s \gtrsim 100$), enclosed by a yellow box, are formed between the structure made of N-terminal sequences ($i = 1 - 150$) and surrounding β-strands forming the barrel. In 23S-rRNA, the locations of the clusters of long-range contacts formed at the interfaces between contact domains are highlighted using different colors on each range of sequences along with the three dimensional structures. **C**. Histogram of the density of long-range contacts calculated for RNA and protein structures in the PDB.

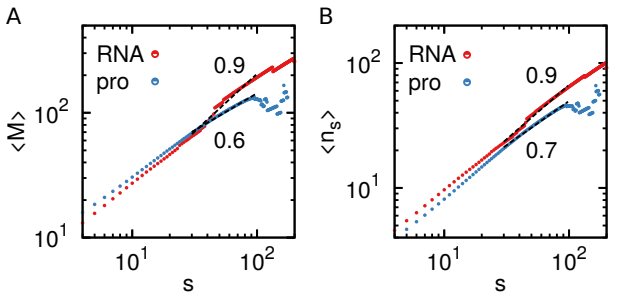

FIG. 3: Chain size frequency weighted number of inter-subchain interactions M (**A**) and the number of surface monomers n_s (**B**) as a function of subchain size s in RNA (red) and proteins (blue).

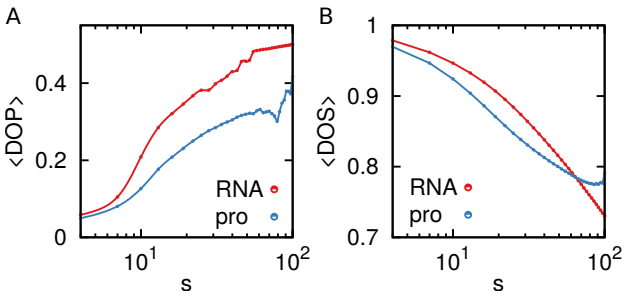

FIG. 4: The mean degree of interpenetration (DOP) and segregation (DOS) as a function of subchain size s in RNA (red) and in proteins (blue).

proteins (Fig. 2), which leads to a smaller exponent, γ.

The number of long-range contacts. The total number of contacts over a given range of s, $s_{\min} < s < s_{\max}$ is considered with $P(s) \approx qs^{-\gamma}$: $n_c(N) = \int_{s_{\min}}^{s_{\max}} (N-s)P(s)ds \approx q\int_{s_{\min}}^{s_{\max}} (N-s)s^{-\gamma}ds$, and hence

$$n_c(N)/q \approx N\left(\frac{s_{\max}^{1-\gamma} - s_{\min}^{1-\gamma}}{1-\gamma}\right) + \left(\frac{s_{\max}^{2-\gamma} - s_{\min}^{2-\gamma}}{2-\gamma}\right). \quad (3)$$

Notably, (i) n_c/q scales linearly with N for both RNA and proteins, regardless of γ value. (ii) The prefactor of n_c/q depends only on γ. For $s_{\min} = 30$ and $s_{\max} = 100$, Eq.3 leads to $n_c^{\gamma=1.1}(N)/q \approx 0.81N + 46$, and $n_c^{\gamma=1.6}(N)/q \approx 0.11N + 6.0$.

Meanwhile, from the plots of $n_c(N)$ using structures in PDB (see Fig. 5), we obtain

$$n_c^{\rm RNA}(N)/q^{\rm RNA} \approx 0.77N + 65$$
$$n_c^{\rm pro}(N)/q^{\rm pro} \approx 0.11N + 4.7, \quad (4)$$

where the prefactors $q^{\rm RNA} \approx 0.48$ and $q^{\rm pro} \approx 4.71$ from the fits to $\langle \overline{P}(s) \rangle$ in Fig. 1 are used. Note that for a given N, $n_c^{\gamma=1.1}(N) > n_c^{\gamma=1.6}(N)$ and $n_c^{\rm RNA}(N) > n_c^{\rm pro}(N)$. Together with other quanti-

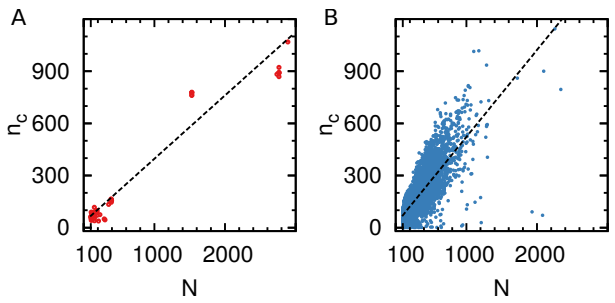

FIG. 5: Scatter plots of the number of contacts for RNA (left) and proteins (right) over the intermediate range with $s_{\min} = 30$ and $s_{\max} = 100$.

ties, $\langle \mathrm{DOP} \rangle$, $\langle \mathrm{DOS} \rangle$, $\langle M(s) \rangle$ and $\langle n_s(s) \rangle$, the number of contacts, $n_c(N)$, calculated here persistently assert that RNA have greater number of long-range contacts than proteins of the same size.

It is of note that the analyses presented in Figs. 3, 4, 5 are different from investigating each macromolecule one by one (Fig. 1) and finding the structure-function relationship. Given that the ensemble in question is the product of evolution, clarifying the difference between two classes of macromolecules (RNA and proteins) is promising as soon as the evolutionary questions are concerned.

DISCUSSION

Due to intramolecular forces stabilizing chain molecule, both native RNA and protein molecules retain compact and space-filling structures, satisfying $R_G \sim N^{1/3}$ [6, 38], which from the polymer physics perspective is regarded as the property of polymers in poor solvent conditions. It is, however, critical to note that the size of a *subchain* surrounded by other subchains should scale as $R(s) \sim s^{1/2}$, which is indeed confirmed for the proteins with $\gamma = 1.5$ (Fig.S5). According to the "Flory theorem" [14, 39], a test chain in a *fully* equilibrated homogeneous semi-dilute or concentrated polymer melt [40], in spherical confinement [41], or even in globule is expected to obey the Gaussian statistics because of the screening of excluded volume interaction or counterbalance between attraction and repulsion [14], thus satisfying $R(s) \sim s^{1/2}$ or $P(s) \sim s^{-3/2}$ (see Supporting Material). The distinct contact probability exponent is highlighted by our analysis that $\gamma \sim 1.0$ for large RNA and $\gamma \sim 1.5$ for small RNA or globular proteins over the intermediate range of $20 \lesssim s \lesssim 100$. Evident from rRNA structure (Fig. 1), subchains of RNA at scales $s > 20$ are assembled into modular contact domains, which are better demarcated in the form of stem-loop helices than proteins, and stitched together through long-range tertiary contacts (Fig. 2A). The evidence of this characteristic architecture of RNA with multi-modular domains is visualized vividly in the form of multiple rupture events in single molecule pulling experiments of *T.* ribozymes [42], while many proteins display a cooperative and effectively all-or-none unfolding under force [30, 43].

What causes the crumpled structures of large RNA at the scale of $20 \lesssim s \lesssim 100$? Here, the statistical rarity of knots in native RNA [44, 45], which is unparalleled by proteins or DNA [34, 46], is worth noting. In general, knots are unavoidable when a long polymer chain ($N \gg N_e \sim 200$ where N_e is the entanglement length [40]) is folded to an equilibrium globule [16, 47]. Topological knot-free constraints inherent to the ring polymers, however, have been shown to organize melts of unconcatenated polymer rings or a single long polymer ring into crumpled globules, preventing entanglements [35, 48]. Since large RNA molecules, assembled by a number of secondary structural elements (hairpin loops, stems), resemble a collection of small and large rings, it can be surmised during the folding process, the knot-free constraints are effectively imposed. The knot-free constraints are more likely applied for RNA because the energy scale associated with secondary structure elements ($\varepsilon^{\mathrm{sec}}$), is in general well separated from that of tertiary interactions ($\varepsilon^{\mathrm{ter}}$), such that $\sum_i \varepsilon_i^{\mathrm{sec}} \gg \sum_k \varepsilon_k^{\mathrm{ter}} \gg k_B T$ [49], which makes secondary structure elements *independently stable*. By contrast, in order to fold, proteins undergo reptation-like process, after the initial collapse [50], which may take place with ease because secondary structure elements of proteins (α-helix, β-sheet) are only marginally stable relative to the thermal energy. If necessary, these motifs can be reassembled into thermodynamically more stable structures.

While local and remote contacts are mixed in the folding nuclei of proteins, the formation of secondary structures in RNA folding usually precedes the formation of tertiary contacts, so that the folding of RNA is hierarchical [2, 51]. Folding under kinetic control produces thermodynamically metastable and kinetically trapped intermediates, which occurs ubiquitously in RNA folding [52], especially in cotranscriptional folding of RNA [53, 54]. A decision, made at an early stage of folding, involved with the formation of independently stable secondary structure elements is difficult to revert although in a worst case scenario, cofactors such as metal-ions [55, 56], metabolites [57], and RNA chaperones [58] still can induce a secondary structure rearrangement. Hence, a more proper way to understand conformational dynamics of a large RNA

molecule with $N \gtrsim 100$ is to consider an ensemble of multiple functional states [59–62] instead of a thermodynamically driven, unique native state. It is noteworthy that RNA secondary structure prediction algorithms which use the strategy of searching the minimum free energy structure [63–65] fail to predict the correct secondary structure when $N \gtrsim 100$, and require the comparative sequence analysis or experimental constraints [66, 67]. This could be ascribed to the consequence of error accumulated in predicting RNA structures with large N, but it is also suspected that the (free) energy minimization principle cannot be extended to account for the folding process of large RNA. The contact statistics of large RNA, $P(s) \sim s^{-1}$, can be used as an additional constraint or guideline for structure prediction.

A situation analogous to the hierarchical folding of large RNA is prevalent in the two-stage membrane protein folding where the insertion of transmembrane (TM) α-helices, guided by translocons, is followed by the post-insertion folding [68, 69]. We indeed find that the contact probabilities of class A G-protein coupled receptors (GPCRs) give $\gamma \approx 1$ (blue circles in the middle panel of Fig. 1). Since $\gamma \approx 1$ means the chain organization of native GPCRs is not in entropy-maximum state, a thermodynamically guided, spontaneous *in vitro* refolding of GPCRs into the native form is expected to be non-permissible. An AFM experiment on an α-helical membrane protein, antiporter ($N \approx 380$), whose γ value we find is ≈ 1.1, could not be refolded to the original form after mechanically unfolded [70]. However, a recent remarkable single molecule force experiment [71] has shown that GlpG, an α-membrane proteins with $N \approx 270$, can reversibly fold in bicelles even after the entire structure including TM helices is disrupted by mechanical forces. Remarkably, we find $\gamma \approx 1.5$ for GlpG. For membrane proteins of known native structures, their γ values can be used to judge whether or not spontaneous *in vitro* refolding is possible.

Since the time required for equilibrium sampling of conformations (τ_{eq}) increases exponentially with the system size (N) as $\tau_{eq} \sim e^N$ [72], signatures of metastability or non-equilibration in chain conformation could be ubiquitous in a macromolecular structure with large N. Through the statistical analysis of structures in PDB, our study puts forward that the present forms of crumpled chain organization with $\gamma \approx 1$ of large native RNA and some classes of proteins are an ineluctable outcome of the folding mechanism under kinetic control.

Our results, based on the structures available in PDB, might be fraught with a possible sample bias since the current structural information available in PDB is limited underrepresenting intrinsically disordered proteins or membrane proteins for proteins, and long non-coding intron RNA (lncRNA) abundant in the cell for RNA [73, 74]. Nevertheless, our general conclusions on the difference in the organization principle between proteins and RNA will still hold even when the database of PDB is further expanded. Especially, we expect that an inclusion of long non-coding RNA structures ($N > 200$), which should be possible in the near future, will make our conclusions more robust since the hierarchical nature of RNA folding process would become more evident for RNA with larger N and reinforce the territorial (crumpled-like) organization in RNA.

ACKNOWLEDGMENTS

We thank the Korea Institute for Advanced Study for providing computing resources (KIAS Center for Advanced Computation, Linux Cluster System) for this work.

* To whom correspondence should be addressed. Email: hyeoncb@kias.re.kr

[1] P. Schuster, W. Fontana, P. F. Stadler, and I. L. Hofacker, Proc.R. Soc. London B: Biological Sci. **255**, 279 (1994).
[2] I. Tinoco Jr. and C. Bustamante, J. Mol. Biol. **293**, 271 (1999).
[3] D. Thirumalai and C. Hyeon, Biochemistry **44**, 4957 (2005).
[4] S. J. Chen and K. A. Dill, Proc. Natl. Acad. Sci. U. S. A. **97**, 646 (2000).
[5] F. Morcos, N. P. Schafer, R. R. Cheng, J. N. Onuchic, and P. G. Wolynes, Proc. Natl. Acad. Sci. U. S. A. **111**, 12408 (2014).
[6] C. Hyeon, R. I. Dima, and D. Thirumalai, J. Chem. Phys. **125**, 194905 (2006).
[7] D. Thirumalai, N. Lee, S. A. Woodson, and D. K. Klimov, Annu. Rev. Phys. Chem. **52**, 751 (2001).
[8] P. R. Langer-Safer, M. Levine, and D. C. Ward, Proc. Natl. Acad. Sci. U. S. A. **79**, 4381 (1982).
[9] T. Cremer and C. Cremer, Nature Rev. Genet. **2**, 292 (2001).
[10] J. Dekker, K. Rippe, M. Dekker, and N. Kleckner, Science **295**, 1306 (2002).
[11] E. Lieberman-Aiden, N. van Berkum, L. Williams, M. Imakaev, T. Ragoczy, A. Telling, I. Amit, B. Lajoie, P. Sabo, M. Dorschner, et al., Science **326**, 289 (2009).
[12] J. Dekker, M. A. Marti-Renom, and L. A. Mirny, Nat. Rev. Genetics **14**, 390 (2013).

[13] J. Zuin, J. R. Dixon, M. I. van der Reijden, Z. Ye, P. Kolovos, R. W. Brouwer, M. P. van de Corput, H. J. van de Werken, T. A. Knoch, W. F. van IJcken, et al., Proc. Natl. Acad. Sci. U. S. A. **111**, 996 (2014).

[14] A. Y. Grosberg and A. R. Khokhlov, *Statistical Physics of Macromolecules* (AIP Press, New York, 1994).

[15] A. Grosberg, S. Nechaev, and E. Shakhnovich, J. Phys. **49**, 2095 (1988).

[16] L. A. Mirny, Chromosome Res. **19**, 37 (2011).

[17] M. Bohn, D. W. Heermann, and R. van Driel, Phys. Rev. E **76**, 051805 (2007).

[18] M. Barbieri, M. Chotalia, J. Fraser, L.-M. Lavitas, J. Dostie, A. Pombo, and M. Nicodemi, Proc. Natl. Acad. Sci. U. S. A. **109**, 16173 (2012).

[19] H. Kang, Y.-G. Yoon, D. Thirumalai, and C. Hyeon, Phys. Rev. Lett. **115**, 198102 (2015).

[20] E. Pyetan, D. Baram, T. Auerbach-Nevo, and A. Yonath, Pure Appl. Chem. **79**, 955 (2007).

[21] Q. Guo, Y. Yuan, Y. Xu, B. Feng, L. Liu, K. Chen, M. Sun, Z. Yang, J. Lei, and N. Gao, Proc. Natl. Acad. Sci. U. S. A. **108**, 13100 (2011).

[22] B. L. Golden, H. Kim, and E. Chase, Nature. Struct. Mol. Biol. **12**, 82 (2005).

[23] A. S. Krasilnikov, Y. Xiao, T. Pan, and A. Mondragón, Science **306**, 104 (2004).

[24] S. Thore, C. Frick, and N. Ban, J. Am. Chem. Soc. **130**, 8116 (2008).

[25] A. D. Ferguson, V. Braun, H.-P. Fiedler, J. W. Coulton, K. Diederichs, and W. Welte, Protein Science **9**, 956 (2000).

[26] L. R. Otterbein, P. Graceffa, and R. Dominguez, Science **293**, 708 (2001).

[27] K. McLuskey, J. Rudolf, W. R. Proto, N. W. Isaacs, G. H. Coombs, C. X. Moss, and J. C. Mottram, Proc. Natl. Acad. Sci. U. S. A. **109**, 7469 (2012).

[28] M. Ormö, A. B. Cubitt, K. Kallio, L. A. Gross, R. Y. Tsien, and S. J. Remington, Science **273**, 1392 (1996).

[29] L. Weaver and B. Matthews, J. Mol. Biol. **193**, 189 (1987).

[30] E. A. Shank, C. Cecconi, J. W. Dill, S. Marqusee, and C. Bustamante, Nature **465**, 637 (2010).

[31] W. Huang, V. Lunin, Y. Li, S. Suzuki, N. Sugiura, H. Miyazono, and M. Cygler, J. Mol. Biol. **328**, 623 (2003).

[32] R. T. Batey, R. P. Rambo, J. A. Doudna, et al., Angew. Chem. Int. Ed. **38**, 2326 (1999).

[33] P. Nissen, J. A. Ippolito, N. Ban, P. B. Moore, and T. A. Steitz, Proc. Natl. Acad. Sci. U. S. A. **98**, 4899 (2001).

[34] R. C. Lua and A. Y. Grosberg, PLoS Comput Biol **2**, e45 (2006).

[35] J. D. Halverson, J. Smrek, K. Kremer, and A. Y. Grosberg, Rep. Prog. Phys. **77**, 022601 (2014).

[36] I. N. Berezovsky, A. Y. Grosberg, and E. N. Trifonov, FEBS Lett **466**, 283 (2000).

[37] A. L. Sanborn, S. S. Rao, S.-C. Huang, N. C. Durand, M. H. Huntley, A. I. Jewett, I. D. Bochkov, D. Chinnappan, A. Cutkosky, J. Li, et al., Proc. Natl. Acad. Sci. U. S. A. **112**, E6456 (2015).

[38] P. J. Flory, *Statistical Mechanics of Chain Molecules*, New York (Interscience Publishers, 1969).

[39] P. J. Flory, J. Chem. Phys. **17**, 303 (1949).

[40] P. G. de Gennes, *Scaling Concepts in Polymer Physics* (Cornell University Press, Ithaca and London, 1979).

[41] A. Cacciuto and E. Luijten, Nano Lett. **6**, 901 (2006).

[42] B. Onoa, S. Dumont, J. Liphardt, S. B. Smith, I. Tinoco, and C. Bustamante, Science **299**, 1892 (2003).

[43] M. Mickler, R. I. Dima, H. Dietz, C. Hyeon, D. Thirumalai, and M. Rief, Proc. Natl. Acad. Sci. U. S. A. **104**, 20268 (2007).

[44] C. Micheletti, M. Di Stefano, and H. Orland, Proc. Natl. Acad. Sci. U. S. A. **112**, 2052 (2015).

[45] A. S. Burton, M. Di Stefano, N. Lehman, H. Orland, and C. Micheletti, RNA Biology **13**, 134 (2015).

[46] J. K. Noel, J. I. Sułkowska, and J. N. Onuchic, Proc. Natl. Acad. Sci. U. S. A. **107**, 15403 (2010).

[47] A. Y. Grosberg, Phys. Rev. Lett. **85**, 3858 (2000).

[48] M. V. Imakaev, K. M. Tchourine, S. K. Nechaev, and L. A. Mirny, Soft matter **11**, 665 (2015).

[49] D. Thirumalai and C. Hyeon, *Non-Protein Coding RNAs* (Springer, 2008), chap. Theory of RNA Folding: From Hairpins to Ribozymes.

[50] D. Thirumalai, J. Phys. I (Fr.) **5**, 1457 (1995).

[51] W. J. Greenleaf, K. L. Frieda, D. A. N. Foster, M. T. Woodside, and S. M. Block, Science **319**, 630 (2008).

[52] D. K. Treiber and J. R. Williamson, Curr. Opin. Struct. Biol. **11**, 309 (2001).

[53] D. Repsilber, S. Wiese, M. Rachen, A. W. Schroeder, D. Riesner, and G. Steger, RNA **5**, 574 (1999).

[54] B. Lutz, M. Faber, A. Verma, S. Klumpp, and A. Schug, Nucleic Acids Res. **42**, 2687 (2013).

[55] M. Wu and I. Tinoco, Jr, Proc. Natl. Acad. Sci. U. S. A. **95**, 11555 (1998).

[56] E. Koculi, S. S. Cho, R. Desai, D. Thirumalai, and S. A. Woodson, Nucleic Acids Res. **40**, 8011 (2012).

[57] R. K. Montange and R. Batey, Annu. Rev Biophys. **37**, 117 (2008).

[58] R. Russell, I. Jarmoskaite, and A. M. Lambowitz, RNA Biology **10**, 44 (2013).

[59] H. Al-Hashimi and N. Walter, Curr. Opin. Struct. Biol. **18**, 321 (2008).

[60] S. V. Solomatin, M. Greenfeld, S. Chu, and D. Herschlag, Nature **463**, 681 (2010).

[61] C. Hyeon, J. Lee, J. Yoon, S. Hohng, and D. Thirumalai, Nat. Chem. **4**, 907 (2012).

[62] C. Hyeon, M. Hinczewski, and D. Thirumalai, Phys. Rev. Lett. **112**, 138101 (2014).

[63] E. Rivas and S. Eddy, J. Mol. Biol. **285**, 2053 (1999), ISSN 0022-2836.

[64] I. Hofacker, Nucleic Acids Res. **31**, 3429 (2003), ISSN 0305-1048.

[65] M. Zuker, Nucleic Acids Res. **31**, 3406 (2003).

[66] R. R. Gutell, J. C. Lee, and J. J. Cannone, Curr. Opin. Struct. Biol. **12**, 301 (2002).

[67] D. Mathews, J. Sabina, M. Zuker, and D. Turner, J. Mol. Biol. **288**, 911 (1999).

[68] J.-L. Popot, S.-E. Gerchman, and D. M. Engelman, J. Mol. Biol. **198**, 655 (1987).

[69] J. U. Bowie, Nature **438**, 581 (2005).

[70] A. Kedrov, C. Ziegler, H. Janovjak, W. Kühlbrandt,

and D. J. Müller, J. Mol. Biol. **340**, 1143 (2004).
[71] D. Min, R. Jefferson, J. Bowie, and T.-Y. Yoon, Nat. Chem. Biol. **11**, 981 (2015).
[72] R. Palmer, Adv. Phys. **31**, 669 (1982).
[73] J. L. Rinn and H. Y. Chang, Annu. Rev. Biochem. **81** (2012).
[74] P. Carninci, T. Kasukawa, S. Katayama, J. Gough, M. Frith, N. Maeda, R. Oyama, T. Ravasi, B. Lenhard, C. Wells, et al., Science **309**, 1559 (2005).
[75] B. Friedman and B. O'Shaughnessy, J. Phys. II **1**, 471 (1991).

SUPPORTING MATERIAL

Extraction of Scaling Exponent γ We obtained the contact probability exponent γ by conducting linear regression on a part of $P(s)$ data that behave as $\sim s^{-\gamma}$ in log-log scale. There are two factors that may affect in determination of γ: (i) d_c, the cut-off distance to define a contact between two residues, affects the overall shape of $P(s)$; (ii) The range of s, $s_{\min} < s < s_{\max}$, to be fitted. Instead of manually tuning the fitting range ($s_{\min} < s < s_{\max}$), we defined a parameter φ ($0 < \varphi < 1$), such that the proportion of fitting range, $(s_{\max} - s_{\min})/N$ where N is the chain length, is at least greater than an allocated threshold value, φ. For instance, if φ is set to 0.3 then the fit is made on more than 30 % of the entire data points. Thus, by fitting $P(s)$ data over all possible pairs of $s_{\min}$ and $s_{\max}$ values which define the range of $(s_{\min}, s_{\max})$ satisfying $(s_{\max} - s_{\min})/N \geq \varphi$, we determine the value of γ from the best fit which gives the smallest standard error relative to the data points.

Fig. S1A shows that the shape of $P(s)$ for 23S-rRNA calculated with different d_c remains effectively identical, giving rise to a similar value of γ: $\gamma = 1.11$ ($d_c = 4$ Å), 1.06 ($d_c = 5$ Å). $p(\gamma)$s for RNA molecules obtained from different d_c are also similar as shown in Fig. S1B.

Next, to study the effect of φ on γ, we set $d_c = 4$ Å and change the value of φ in the fit. We obtain $\gamma = 1.11$ for $\varphi = 0.3$, and $\gamma = 1.01$ with $\varphi = 0.4$ (see Fig. S2A). Fig. S2B also shows that $p(\gamma)$ with different φ are comparable. Analysis applied to protein shows similar results. A series of comparisons in Figs.S1 and S2 indicate that the average value of γ is insensitive to the parameters around the value we have chosen.

In addition, the overall shapes of $p(\gamma)$ and $\langle \overline{P}(s) \rangle$ are insensitive to the two threshold values of sequence similarity (90 and 30 %), which we imposed to select a set of non-homologous proteins (Fig. S3).

We analyzed 186 RNA and 16633 individual proteins whose size satisfies $N \geq 50$, available in PDB as of September 2015. Distributions of γ obtained from the optimal linear fittings on $\log_{10} P(s)$ versus $\log_{10} s$ with a correlation coefficient greater than 0.9 are presented in Fig.1A with $\varphi = 0.3$, $d_c = 4$ Å for both RNAs and proteins. To highlight the robustness of our result presented in Fig.1A (γ vs. N plot), we specified the 95 % confidence interval of γ values using error-bar to each data point in Fig. S4.

Contact probability between two sites of a polymer In general, the contact probability of two sites in polymer chain is determined by the volume available for the subchain ending with the two sites,

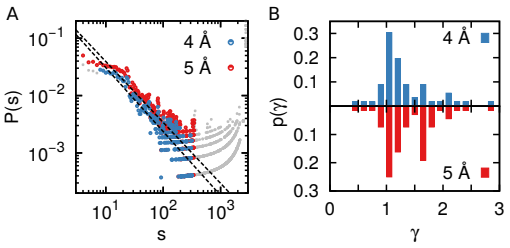

FIG. S1: (A) The contact probability versus sequence distance of 23S rRNA (PDB entry 2O45) with a cut-off distance of contacting d_c of value 4 Å (blue) and 5 Å (red). (B) Distributions of γ in RNA monomers with d_c of 4 Å and 5 Å.

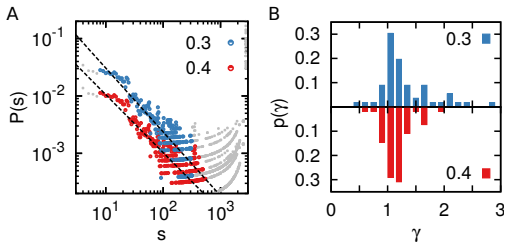

FIG. S2: (A) The contact probability versus sequence distance of 23S rRNA (PDB entry 2O45) with a minimum fraction of all data points used for fitting φ of 0.3 (blue) and 0.4 (red). The data points for $\varphi = 0.4$, as well as the fitted dashed line, are shifted downwards for visual comparison. (B) Distributions of γ in RNA monomers of φ 0.3 and 0.4.

$[R(s)]^d$, with normalization condition $\int P_s(r) d^d r = 1$ [14, 40]:

$$P_s(r) = \frac{1}{R(s)^d} \varphi\left(\frac{r}{R(s)}\right) \xrightarrow{r \ll R(s)} P(s) = \frac{1}{R(s)^d}\left(\frac{r}{R(s)}\right)^g, \quad \text{(S1)}$$

where r is the contact distance, $R(s)$ is the size of polymer made of s monomers, d is the dimensionality, and g is the correlation hole exponent. With $R(s) \sim s^\nu$ (see Fig. S5), we obtain the scaling relationship of contact probability, $P(s) \sim s^{-\nu(d+g)}$.

(i) When the excluded volume interaction is fully screened, a test chain (or subchain over a certain length) is ideal. In this case, $\varphi(x) \sim e^{-3x^2/2}$. Thus, the correlation hole exponent $g = 0$ [75] and $R \sim s^\nu$ with $\nu = 1/2$, which leads to $P(s) \sim s^{-\nu d} \sim s^{-3/2}$.

(ii) If the chain adopts an *effectively homogeneous* space-filling configuration, but the interaction between monomers is weak and the excluded volume interaction

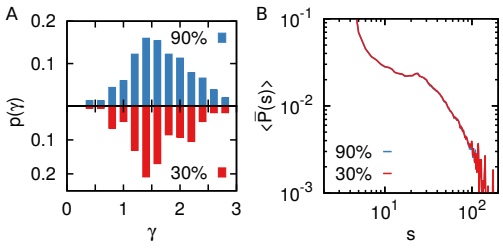

FIG. S3: Effects of imposing different threshold value for the sequence similarity of 90 % and 30 % to the protein structure database to compute $p(\gamma)$ and $\langle \overline{P}(s) \rangle$. No qualitative difference is found in the results.

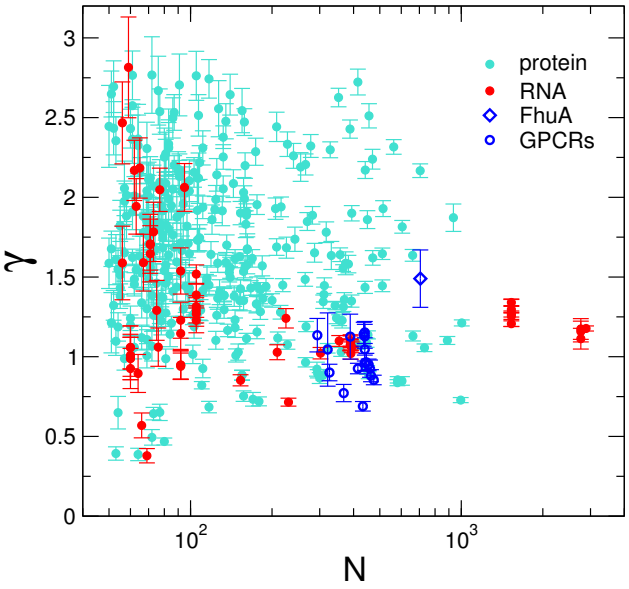

FIG. S4: Scatter plot of γ versus N for RNA (red) and proteins (cyan) with error bars (95 % confidence interval) for γ values.

is still fully screened as in a concentrated melt, then $g = 0$, $d = 3$, and $\nu = 1/3$, which leads to $P(s) \sim s^{-1}$.

(iii) If the chain organization is *inhomogeneous* leading to an anisotropic arrangement because of strong monomer-monomer interactions [37], which for the case of RNA leads to formation of independently stable helices, then $R(s)$ still satisfies $R(s) \sim s^{1/3}$ but the effective dimensionality of the sampling space ($d_{\rm eff}$) would be less than 3. Thus, $P(s) \sim s^{-d_{\rm eff}/3}$, and $\gamma = d_{\rm eff}/3 < 1$, which accounts for the contact probability exponent smaller than 1.

(iv) Note that when the subchain interactions (repulsion and attraction) are screened ($g = 0$), $P(s)$ and $R(s)$ are related as $P(s) \sim R(s)^{-d}$. This relationship particularly holds good for intermediate range of s: $P(s) \sim s^{-3/2} \leftrightarrow R(s) \sim s^{1/2}$ (ideal chain) and $P(s) \sim s^{-1} \leftrightarrow R(s) \sim s^{1/3}$ (crumpled chain) (see Fig. S5). The scaling exponent of 3/5 at $s < 10$ in Fig. S5 is due to the volume exclusion interaction at short range s.

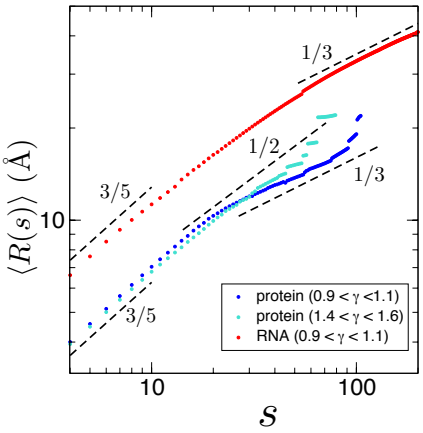

FIG. S5: Mean radius of gyration of subchain as a function of subchain length s for proteins and RNA that display contact probability exponent in a specified range of γ. The structures in the specified range of γ were collected from Fig. 1 and their $R(s)$s were calculated.

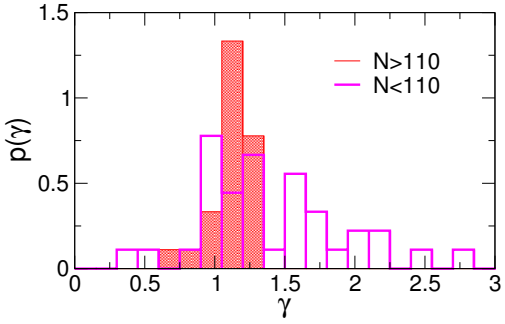

FIG. S6: Distribution of γ value for RNA with $N > 110$ and $N < 110$. $\gamma^{\rm RNA}_{N>110} = 1.12 \pm 0.14$ and $\gamma^{\rm RNA}_{N<110} = 1.41 \pm 0.53$.

2M58	2MIY	1FIR	6TNA	1EHZ	1TRA	4TRA	1TN1
1TN2	3TRA	2TRA	3BBV	1VTQ	4PQV	3A3A	3CW6
2HOP	1I9V	3L0U	2K4C	3D2G	4NYD	2HOM	3GX6
2GIS	3GX2	3IQN	4B5R	2YDH	4RZD	3F2Q	3F2W
3F30	3F2X	3F2T	3F2Y	1U9S	3DHS	1Y0Q	4C4Q
2A2E	3BWP	4FAX	4E8P	4E8R	4E8Q	4E8N	4DS6
4E8M	4FAQ	3J2B	3J2H	3J2D	2YKR	3J28	3J2A
2O45	2O43	2O44	1C2W				

TABLE I: PDB entries of RNA analyzed in Fig. 1.

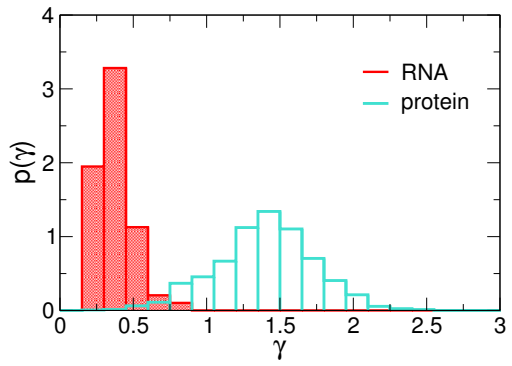

FIG. S7: Distribution of contact probability exponent calculated for the short range of s, $s < 20$. $\gamma^{\mathrm{RNA}} = 0.38 \pm 0.13$ and $\gamma^{\mathrm{pro}} = 1.40 \pm 0.33$.

2MGW	2JY5	2CR8	2RRU	2KAK	2DAH	2EPS	1JJR
1KMX	2KQB	1YSM	2ECM	2KMU	1KFT	2KPI	2M8E
2K2T	2REL	2YSD	2L4E	2MWR	2YRG	3GOH	1Z60
2KKJ	1A7I	1VYX	2M2F	2JXD	2DAL	3WIT	2M9W
2YSJ	1UEO	1AA3	4A3N	1WG2	2D8U	1WFH	1HYI
1BW5	2DZL	1X4P	1VFY	1X4W	1HTA	1SF0	1H0Z
2EA6	2MFK	2DI0	2EWT	2RMR	3H33	1RIY	4TXA
2DA7	2LGW	2JVG	1X61	1WEE	1X4K	2DJB	4P3V
2CT5	2LEK	2HI3	1G33	2EP4	1NEQ	1APJ	1WFP
2JXW	2KW9	1SIG	2M4G	2LT1	1WYS	1X68	2ENN
2E6S	2D9H	2ECT	1E4U	1JQ0	1J3C	1MJ4	4U12
2MLB	1UHC	2CR7	1KDU	1QRY	1X3H	2CSY	2ECL
1RWJ	2LDR	4CIK	3J0R	1UHA	4EIF	1X63	2DOE
2LQL	1CC5	1XFE	2L0S	3CP1	3ZJ1	3BT4	2LRQ
1IPG	2Q18	4IYL	2ECW	2LV2	1LMJ	1ABA	1C9F
1F1F	2CT2	1C6R	1FP0	2KW1	4GPS	1CTJ	2M5W
1Y02	2D8Y	2E6R	1WEO	2CS3	1FBR	2LGX	2LGP
2MIQ	1SJ6	1WIA	2JSN	2DMD	2VTK	3PO8	1OPC
2YRE	2LGV	1T1D	3H6N	1JHG	4BGC	2OA4	2CQK
2CTK	3GCE	2K4J	3DQY	1X0T	2JVL	1HKF	2CS8
3O8V	3DVI	2CTW	4EEU	2MLK	1ZOX	2XXC	2EO3
4TVM	2IVW	2LW4	4HWM	2KQR	2JXN	2HC5	1T6A
4ZBH	1UJX	2MMZ	2LHT	1JUG	2RA9	2XWS	1G3P
2QYZ	2FYG	3O5E	2ES0	4NAZ	3E2I	1DQG	1VSR
1KQW	1E29	2FVV	3W9K	1NL1	1WK0	1XN5	2IN0
2NWF	2L5Q	2P0B	2MO5	3ZUI	2HNA	2JY9	4MYM
3N9D	2N48	4M4Z	3FME	1ENV	2D37	2XB3	1ZND
4GNY	4LD1	3UF4	1D7P	1EW3	3OUQ	1E88	2LFU
2KIG	2KFU	1KLO	3NZM	2M47	4JHG	1RL6	3TXO
2LZM	2NN5	3W9R	2CP6	4F47	1EH6	1CDY	2R6V
3K21	3WJT	1WV3	4M6T	2D5M	3KBG	1J3G	1EJE
1JM1	3TFM	4QA8	1HXN	4E1B	4IT3	4JZC	1EMA
2K18	3HBK	3NO3	4PQ0	2PNN	1LVA	3LTI	4JS8
4DWO	2A1L	4NW4	3V75	5BN7	1DUW	3JRP	2QLU
2LQW	4X36	2HES	4GGC	4GGA	4V16	4AA8	2FGQ
4AF8	1VPR	2PMN	2XE1	2ASI	2ZYL	1T6E	3BA0
1J6Z	4QDC	4GQ1	1FEP	3GRE	4UQE	4MSX	3R1K
3ACP	2DH2	4COT	3DWO	1QCF	1FMK	1W52	1DQ3
1G0D	3K5W	2OBD	4NOX	4FWW	2E84	1Z1N	4AW7
1XEZ	4TLW	1PI6	4UMW	4BBJ	3OKT	1QFG	4MHC
2OAJ	4UP5	1HN0	3KLK				

TABLE II: PDB entries of proteins analyzed in Fig. 1.

2JX9	1ISR	2LNL	2RH1	2YDV	2ZIY	3C9L	3EHS
3EML	3N94	3OE6	3RZE	3UON	3V2Y	3VW7	4DKL
4EJ4	4F11	4IB4	1QJQ				

TABLE III: PDB entries of GPCRs analyzed in Fig. 1.